Scientific Reports

https://doi.org/10.1038/s41598-026-39649-3

Article in Press

Cold inducible RNA binding protein promotes fibroblast activation and its inhibition represents a potential therapeutic target in pulmonary fibrosis

Received: 22 June 2025

Accepted: 6 February 2026

Published online: 11 February 2026

Cite this article as: Mochizuka Y., Hozumi H., Watanabe H. *et al.* Cold inducible RNA binding protein promotes fibroblast activation and its inhibition represents a potential therapeutic target in pulmonary fibrosis. *Sci Rep* (2026). https://doi.org/10.1038/s41598-026-39649-3

Yasutaka Mochizuka, Hironao Hozumi, Hirofumi Watanabe, Atsuki Fukada, Hyogo Naoi, Yusuke Inoue, Hideki Yasui, Yuzo Suzuki, Masato Karayama, Kazuki Furuhashi, Noriyuki Enomoto, Tomoyuki Fujisawa, Naoki Inui & Takafumi Suda

Cold inducible RNA binding protein promotes fibroblast activation and its inhibition represents a potential therapeutic target in pulmonary fibrosis

Yasutaka Mochizuka, M.D.[1], Hironao Hozumi, M.D., Ph. D.[1*], Hirofumi Watanabe, M.D., Ph. D.[1], Atsuki Fukada, M.D., Ph. D.[1], Hyogo Naoi M.D., Ph. D.[1], Yusuke Inoue, M.D., Ph. D.[1], Hideki Yasui, M.D., Ph. D.[1], Yuzo Suzuki, M.D., Ph. D.[1], Masato Karayama, M.D., Ph. D.[1], Kazuki Furuhashi, M.D., Ph. D.[1], Noriyuki Enomoto, M.D., Ph. D.[1], Tomoyuki Fujisawa, M.D., Ph. D.[1], Naoki Inui, M.D., Ph. D.[1,2], Takafumi Suda, M.D., Ph. D.[1]

Affiliations:

[1] Second Division, Department of Internal Medicine, Hamamatsu University School of Medicine, 1-20-1 Handayama Higashiku, Hamamatsu 431-3192, Japan

[2] Department of Clinical Pharmacology and Therapeutics, Hamamatsu University School of Medicine, 1-20-1 Handayama Higashiku, Hamamatsu 431-3192, Japan

Corresponding author: Hironao Hozumi, M.D., Ph. D.

Second Division, Department of Internal Medicine, Hamamatsu University School of Medicine, 1-20-1 Handayama Higashiku, Hamamatsu 431-3192, Japan

Email: hozumi@hama-med.ac.jp; Tel: +81(53)435-2263; Fax: +81(53)435-2354

ORCID ID: 0000-0001-5439-1543

ABSTRACT

Pulmonary fibrosis is a fatal interstitial lung disease marked by irreversible lung structure destruction. Understanding its molecular mechanisms is essential. Cold-inducible RNA-binding protein (CIRBP), a stress-responsive protein, stabilizes mRNA intracellularly and also acts extracellularly. We previously demonstrated that CIRBP is highly expressed in fibrotic lesions of idiopathic pulmonary fibrosis patients, with elevated serum levels correlating with disease progression and poor prognosis. However, its role in fibrosis remains unclear. We investigated CIRBP's function using an in vivo bleomycin (BLM)-induced pulmonary fibrosis mouse model via intratracheal administration and an in vitro model with primary lung fibroblasts. CIRBP expression was markedly upregulated in the fibrotic regions of BLM-treated wild-type (WT) mice. *CIRBP*-deficient mice showed improved survival, reduced fibrosis, lower hydroxyproline content, and decreased expression of α-SMA and fibronectin. Therapeutic administration of C23, a CIRBP-derived inhibitory peptide, significantly suppressed fibrosis and improved survival in WT mice. In vitro, recombinant CIRBP promoted collagen secretion, fibroblast proliferation, and cell migration, which were inhibited by C23. Mechanistically, CIRBP-induced IL-6 production via TLR2 and TLR4, leading to fibroblast activation through autocrine signaling. These effects were suppressed by C23, TLR2/4 inhibitors, or IL-6 neutralization. Our findings identify CIRBP as a novel profibrotic factor and therapeutic target in pulmonary fibrosis.

Keywords: CIRP, fibroblast, Interleukin-6, Toll-like receptor, lung fibrosis, bleomycin

INTRODUCTION

Pulmonary fibrosis is a progressive and fatal form of interstitial lung disease (ILD), characterized by irreversible scarring of the lung parenchyma. It can result from idiopathic causes, autoimmune diseases, or exposure to environmental factors (1-3). Idiopathic pulmonary fibrosis (IPF), the most common ILD, has a median survival of 3–4 years (1). The pathogenesis of pulmonary fibrosis involves repeated alveolar epithelial injury, abnormal fibroblast activation, myofibroblast differentiation, and excessive collagen deposition. These events are driven by mechanisms such as oxidative stress, ER stress, and dysregulated apoptosis (4). Recently, innate immune responses and damage-associated molecular patterns (DAMPs) have been implicated in disease progression (5-7). Currently, two antifibrotic agents, pirfenidone and nintedanib, are approved for IPF and have been shown to slow disease progression (1); however, they have proved unsuccessful in significantly improving survival, thereby underscoring the need for more effective therapies.

Cold-inducible RNA-binding protein (CIRBP) is a stress-responsive molecule whose expression is upregulated under stressful conditions, such as cold exposure, hypoxia, and ultraviolet radiation (8). CIRBP is widely expressed in various cells and tissues, particularly in the brain, heart, testes, and lungs, and is primarily localized in the nucleus, where it functions as an RNA chaperone that stabilizes mRNA (9). In addition, CIRBP can be secreted extracellularly, acting as a DAMP and exerting diverse physiological effects (10). Our previous study demonstrated that CIRBP is highly expressed in fibrotic lesions of IPF lungs and that elevated serum CIRBP levels are significantly associated with deteriorating lung function and poor prognosis (11). These findings suggest a potential role for CIRBP in the progression and prognosis of IPF. A recent study reported that genetic deletion of *CIRBP* or its competitive inhibition using a CIRBP-derived peptide ameliorated fibrosis in a bleomycin (BLM)-induced mouse model via subcutaneous injection (12). However, the subcutaneous

administration method used in the study is not considered standard according to the official American Thoracic Society workshop, and the therapeutic effects of CIRBP have not yet been evaluated using intratracheal (IT) administration via direct instillation or oropharyngeal aspiration (OA), which are recommended as preclinical models for therapeutic assessment (13). Furthermore, the expression of CIRBP in lung tissue, its impact on survival in BLM-treated mice when deficient or inhibited, and its direct role in fibroblasts—the central effector cells in fibrosis—have not been elucidated so far.

In this study, we used a BLM-induced pulmonary fibrosis mouse model via IT administration using the OA method to evaluate CIRBP expression in lung tissue and to assess the therapeutic effects of CIRBP deficiency or inhibition on fibrosis and survival. Additionally, we conducted in vitro analyses using primary cultured mouse lung fibroblasts to investigate the molecular pathways through which CIRBP may contribute to fibrosis and to determine whether its inhibition exerts antifibrotic effects.

MATERIALS AND METHODS

Mice

Male C57BL/6 mice (10–12 weeks old) were purchased from Nippon SLC (Japan SLC, Shizuoka, Japan). CIRBP-deficient mice (*CIRBP*$^{-/-}$ mice) were purchased from the Laboratory Animal Resource Bank, National Institutes of Biomedical Innovation, Health and Nutrition (14) and bred in our facility at Hamamatsu University School of Medicine. All animal experiments were approved by the Animal Care and Use Committee of Hamamatsu University School of Medicine (Approval number: 2022005), and all methods were carried out in accordance with the relevant guidelines and regulations. This study is reported in accordance with the ARRIVE guidelines (https://arriveguidelines.org).

Mouse Model of BLM-Induced Lung Fibrosis

A murine model of pulmonary fibrosis was established by the intratracheal instillation of BLM (Nippon Kayaku, Tokyo, Japan) via OA on day 0. The mice were euthanized on day 21 after intratracheal administration for lung tissue analysis. Mice were anesthetized by intraperitoneal injection of ketamine (100 mg/kg) and xylazine (10 mg/kg) and euthanized by exsanguination under deep anesthesia. Phosphate-buffered saline (PBS) was administered to the controls. The mice were monitored daily and euthanized at a predetermined humane endpoint if they exhibited marked weight loss (body weight ≤ 15 g). BLM was freshly prepared in sterile PBS at concentrations of 0.5 or 1.0 U/mL and administered under anesthesia as described below. For the survival analysis, BLM was administered to mice at a dose of 2 U/kg body weight. However, this dose caused some mice to meet the criteria for humane endpoint euthanasia within 21 days, prompting the use of a lower dose (1 U/kg body weight) for lung tissue analysis.

C23 Peptide Treatment

The C23 peptide (sequence: GRGFSRGGGDRGYGG) was synthesized by GenScript (Piscataway, NJ, USA). C23 is a 15-amino acid peptide derived from CIRBP, known to have a high affinity for the TLR4-MD2 complex, and has been suggested to competitively inhibit CIRBP binding (15). For the C23 treatment experiments, mice from the BLM-treated and control groups received once-daily intraperitoneal injections of either C23 peptide (200 μg/mouse, total volume 200 μL) or placebo (PBS, 200 μL) on days 7–11 and 14–18.

Histopathological Analysis of the Lung Tissues

The lungs were fixed in 4% paraformaldehyde and embedded in paraffin. Lung sections were stained with hematoxylin and eosin and Masson’s trichrome. The severity of pulmonary

fibrosis was assessed using Ashcroft scores (16). Immunohistochemical staining was performed using an anti-CIRBP antibody (2.5 ng/mL; ab106230, Abcam, Cambridge, UK) or an isotype IgG control (2.5 ng/mL; ab37373, Abcam) to assess CIRBP expression.

Hydroxyproline Assay

The pulmonary hydroxyproline content in BLM-treated mice was quantified using a hydroxyproline assay kit (QuickZyme Biosciences, Leiden, The Netherlands), following the manufacturer's instructions.

Isolation and Enrichment of Primary Lung Fibroblasts

Lungs were perfused with PBS, minced into small fragments, and enzymatically digested using collagenase type II (2.0 mg/mL; Roche, Basel, Switzerland) and DNase I (100 µg/mL; Roche) in RPMI 1640 medium at 37°C for 30 minutes. The digested tissue was filtered through 70-µm cell strainers to obtain single-cell suspensions. Viable cells were isolated by centrifugation and resuspended in staining buffer (Hank's Balanced Salt Solution supplemented with 2% fetal calf serum [FCS], 1% penicillin–streptomycin, and 1% HEPES). To enrich fibroblasts, single cells were incubated with fluorophore-conjugated antibodies for 30 minutes at 4°C and then washed twice with the staining buffer. The following antibodies were used: APC-conjugated anti-CD45 (clone 30-F11), anti-TER-119 (clone TER-119), anti-CD324 (clone DECMA-1), anti-CD31 (clone 390), and anti-CD146 (clone ME-9F1), each diluted 1:150; APC-conjugated anti-LYVE-1 (clone 223322, R&D Systems) diluted 1:60; and PE-conjugated anti-CD140a (PDGFRα, clone APA5) diluted 1:50. Dead cells were excluded using propidium iodide staining. Flow cytometric sorting was performed on a MoFlo Astrios EQ cell sorter (Beckman Coulter, Brea, CA, USA). Fibroblasts were defined as lineage-negative ($CD45^-$, $TER\text{-}119^-$, $CD324^-$, $CD31^-$, $CD146^-$, $LYVE\text{-}1^-$) and $PDGFR\alpha^+$ ($CD140a^+$)

cells (**Supplementary Figure 1**). The sorted cells were immediately collected into complete Dulbecco's modified Eagle's medium (DMEM) containing 10% FCS and used for subsequent culture or assays.

Culture and Treatment of Primary Lung Fibroblasts

Primary lung fibroblasts isolated as described above were cultured in DMEM containing 10% FCS and 1% penicillin–streptomycin at 37°C in 5% CO_2. The medium was replaced every 3 days, and cells at passages 3–6 were used for all subsequent experiments.

RNA Isolation and RNA Sequencing

Primary lung fibroblasts were seeded at a density of 1.0×10^6 cells per 10-cm dish. After 24 h of incubation in DMEM containing 10% FCS, the medium was replaced with DMEM containing 0.1% FCS for an additional 24 h to induce serum starvation. Following starvation, the cells were treated with recombinant mouse CIRBP (rmCIRBP) (1.0 μg/mL; CUSABIO, Wuhan, China) or vehicle control in DMEM containing 0.1% FCS for 24 h (n = 3 per condition). Total RNA was then extracted using TRIzol Reagent (Invitrogen, Carlsbad, CA, USA) according to the manufacturer's instructions. RNA sequencing was performed using the Illumina NovaSeq 6000 system, and all data analysis was outsourced to Rhelixa Inc. (Tokyo, Japan). RNA sequencing (RNA-seq) and all subsequent analyses were conducted in a single batch to avoid potential batch effects. The complete datasets are available in the Gene Expression Omnibus database (https://www.ncbi.nlm.nih.gov/geo/) under accession number **GSE294583**.

PCR

Primary lung fibroblasts were seeded, cultured, and serum-starved as described above. Cells were treated with vehicle control, rmCIRBP (1.0 μg/mL), or TGF-β (2.0 ng/mL; 7666-MB, Bio-Techne, Minneapolis, MN, USA) for 24 h, followed by total RNA extraction. Complementary DNA was synthesized from 100 ng of total RNA using the ReverTra Ace® qPCR RT Master Mix (Toyobo, Osaka, Japan) in accordance with the manufacturer's instructions. Quantitative real-time PCR (qPCR) was performed using the THUNDERBIRD® SYBR® qPCR Mix (Toyobo) and the QuantStudio 3 Real-Time PCR System (Thermo Fisher Scientific, Waltham, MA, USA). Relative gene expression levels were calculated using the ΔΔCt method with *Actb* as the internal control. The mouse-specific primers used were as follows: *Acta2*, forward 5'-TGTGCTGGACTCTGGAGATG-3' and reverse 5'-GAAGGAATAGCCACGCTCAG-3'; *fibronectin 1 (Fn1)*, forward 5'-GAAGCAACGTGCTATGACGA-3' and reverse 5'-ATCTAGCGGCATGAAGCACT-3'; and *Actb*, forward 5'-AAGGCCAACCGTGAAAAGAT-3' and reverse 5'-GTGGTACGACCAGAGGCATA-3'.

Western Blot Analysis

Lung tissues were collected on day 21 after intratracheal administration. Total protein was extracted from the right middle lobe using a lysis buffer consisting of 50 mM Tris-HCl (pH 7.6), 1% Nonidet P-40, 0.5% sodium deoxycholate, 150 mM NaCl, and 0.1% SDS. Protein concentrations were measured using the Pierce BCA Protein Assay Kit (Thermo Fisher Scientific). Equal amounts of protein were subjected to SDS-PAGE and transferred onto a polyvinylidene difluoride membrane (Merck, Rahway, NJ). Protein bands were visualized using an enhanced chemiluminescence reagent (ECL Prime, Cytiva) and the amount of protein on the immunoblots was quantified using the ChemiDoc Touch Imaging System (BioRad Laboratories, Philadelphia, PA). The antibodies used for western blotting included

anti-CIRBP (1:1000; ab246510, Abcam), anti-α-smooth muscle actin (α-SMA) (1:1000; #19245, Cell Signaling Technology, Danvers, MA, USA), anti-fibronectin (1:10000; ab45688, Abcam), and anti-β-actin (1:1000; 60008-1-Ig, Proteintech, Rosemont, IL, USA). Primary lung fibroblasts were seeded at a density of 6.0×10^5 cells per 6-cm dish. After 24 h of incubation in DMEM containing 10% FCS, the medium was replaced with DMEM containing 2.0% FCS, and the cells were treated with vehicle control, rmCIRBP (1.0 μg/mL), or TGF-β (2.0 ng/mL). After 5 days of treatment, western blotting was performed using the same protocol described for lung tissues. The same primary antibodies (anti-α-SMA, anti-fibronectin, and anti-β-actin) were used as described above.

Enzyme-Linked Immunosorbent Assay (ELISA)

Primary lung fibroblasts were seeded in a 12-well plate (1.0×10^5 cells per well). After 24 h of incubation in DMEM containing 10% FCS, the medium was replaced with DMEM containing 0.1% FCS for 24 h (serum starvation). Following starvation, the cells were treated with vehicle control, rmCIRBP (1.0 μg/mL), C23 (0.1 μg/mL), TLR4 inhibitor (2.76 μM; CLI-095, tlrl-cli95-4, InvivoGen, San Diego, CA, USA), TLR2 inhibitor (100 μM; TL2-C29, inh-c29, InvivoGen), or combinations thereof. After 24 h of treatment, cytokine concentrations in the culture supernatants were quantified using the arigoPLEX® Mouse Proinflammatory Cytokine Multiplex ELISA Kit and the arigoPLEX® Mouse Fibrotic Marker Multiplex ELISA Kit (arigo Biolaboratories Corp., Taiwan) according to the manufacturer's instructions.

Collagen Concentration Assay

Primary lung fibroblasts were seeded at a density of 1.0×10^5 cells per well in a 12-well plate. After 24 h of incubation in DMEM containing 10% FCS, the medium was replaced with

DMEM containing 2.0% FCS. The cells were then treated with vehicle control, rmCIRBP (1.0 μg/mL), C23 (0.1 μg/mL), anti-IL-6 antibody (15 μg/mL; Thermo Fisher Scientific), TLR4 inhibitor (2.76 μM), TLR2 inhibitor (100 μM), TGF-β (2.0 ng/mL), or combinations thereof. After 5 days of treatment, the concentration of acid-soluble collagen in the culture supernatant was quantified using the Sircol Soluble Collagen Assay Kit (Biocolor Life Science Assays, UK) according to the manufacturer's instructions (1 mL of culture supernatant was used for each assay).

Primary Lung Fibroblast Proliferation Assay

Primary lung fibroblasts were seeded at 5,000 cells per well in a 96-well plate with DMEM containing 10% FCS for 24 h. Subsequently, the medium was replaced with DMEM containing 0.1% FCS for another 24 h (serum starvation). Next, the cells were treated with vehicle control, rmCIRBP (1.0 μg/mL), PDGF-BB (20 ng/mL; SRP3229, Sigma-Aldrich), C23 (0.1 μg/mL), anti-IL-6 antibody (15 μg/mL), TLR4-inhibitor (2.76 μM), TLR2-inhibitor (100 μM), or combinations thereof. Cell proliferation was assessed using a Cell Counting Kit-8 (Dojindo Molecular Technologies, Kumamoto, Japan) according to the manufacturer's instructions at 0, 24, and 48 h.

Cell Migration Assay

Cell migration was evaluated using a stencil-based wound-healing model (Stencell Allegro, Idylle, Paris, France) according to the manufacturer's instructions. Primary mouse lung fibroblasts were seeded at a density of 1.0×10^4 cells per well into Stencell devices placed on 6-well culture plates. After allowing the cells to attach and spread for 1–2 h at 37°C in 5% CO_2, 2 mL of DMEM containing 10% FCS was gently added to each well, and cultures were maintained until they reached approximately 90% confluence. Prior to initiating migration,

cells were serum-starved overnight in DMEM containing 0.1% FCS. The Stencell barriers were then carefully removed using sterile tweezers to create cell-free gaps. Immediately thereafter, the medium was replaced with 2 mL of DMEM containing 0.1% FCS and the designated treatments. Treatment groups consisted of vehicle control, rmCIRBP (1 μg/mL), C23 peptide (0.1 μg/mL), rmCIRBP plus C23, and TGF-β (2 ng/mL). Cell migration into the gap was monitored by phase-contrast microscopy at 0 h and 24 h. Wound areas were quantified using ImageJ software (NIH, USA), and the percentage of wound closure was calculated as: (initial wound area − wound area at 24 h) / initial wound area × 100%.

Collagen Gel Contraction Assay

Collagen gel contraction was assessed using a Collagen-based Cell Contraction Assay Kit (Cell Biolabs, CBA-201) according to the manufacturer's protocol. Primary mouse lung fibroblasts were suspended in DMEM containing 2% FCS at a density of 2×10^5 cells per well. The cell suspension was mixed with the collagen gel working solution on ice at a 1:4 ratio to achieve a final collagen concentration of 2.4 mg/mL. The collagen–cell mixture was dispensed into a 24-well plate and incubated for 1 h at 37°C to allow gel polymerization. After gel formation, 1.0 mL of DMEM containing 2% FCS and the designated treatments was added to each well. Treatment groups included vehicle control, rmCIRBP (1 μg/mL), C23 peptide (0.1 μg/mL), rmCIRBP plus C23, and TGF-β (2 ng/mL). Gels without cells served as negative controls. After 48 h of incubation at 37°C in 5% CO_2, collagen gels were gently released from the well edges using a sterile spatula to initiate contraction. Images of the gels were captured immediately after release (0 h) and after 24 h using a digital imaging system (ChemiDoc Touch, Bio-Rad). Gel areas were measured using ImageJ software (NIH, USA), and the contraction index (%) was calculated as: (gel area at 24 h / gel area at 0 h) × 100%.

Statistical Analysis

Student's t-tests and one-way analysis of variance (ANOVA) with Tukey's multiple comparison tests were used for comparisons among groups. Survival was assessed using Kaplan–Meier curves and log-rank tests. A P-value of <0.05 was considered significant. All data are presented as means ± the standard error of the mean (SEM). Statistical analyses were performed using GraphPad Prism version 9.3.1 (GraphPad Software).

RESULTS

Comparison of WT and CIRBP$^{-/-}$ Mice in the BLM-Induced Pulmonary Fibrosis Model

We compared the WT and *CIRBP*$^{-/-}$ mice to investigate the role of CIRBP in the development of pulmonary fibrosis (**Figure 1A**). The *CIRBP*$^{-/-}$ mice exhibited significantly improved survival compared to the WT mice following BLM administration (**Figure 1B**). Histological evaluation of lung tissues on day 21 demonstrated that the BLM-treated *CIRBP*$^{-/-}$ mice developed significantly less pulmonary fibrosis than the BLM-treated WT mice, as evidenced by the lower Ashcroft scores (**Figure 1C**). The hydroxyproline content, a quantitative indicator of collagen accumulation, was also significantly reduced in the lungs of BLM-treated *CIRBP*$^{-/-}$ mice compared to those of BLM-treated WT mice (**Figure 1D**). Western blot analysis was performed to assess CIRBP expression and fibrosis-related protein levels in the lungs. In WT mice, CIRBP expression in the lungs was weak under control conditions but markedly increased following BLM administration; in contrast, CIRBP was undetectable in the control and BLM-treated *CIRBP*$^{-/-}$ mice, confirming the knockout status (**Figure 1E**). Furthermore, the expression levels of fibrotic markers, including α-SMA and fibronectin, were significantly lower in the BLM-treated *CIRBP*$^{-/-}$ mice than in the BLM-treated WT mice (**Figure 1F–G**).

Taken together, these results indicate that CIRBP expression is upregulated during BLM-induced pulmonary fibrosis, and *CIRBP* deficiency leads to improved survival and attenuated fibrosis, suggesting a critical role for CIRBP in lung fibrosis.

Pulmonary Distribution of CIRBP Expression

In our mouse model experiments, we confirmed a marked upregulation of CIRBP expression in the lungs of BLM-treated WT mice. However, the spatial distribution of CIRBP in the lungs remains unclear. Immunohistochemical staining on lung sections from PBS-treated (control) and BLM-treated WT mice was conducted to assess the localization of CIRBP expression in lung tissue. CIRBP was mainly expressed around the airways in the control lungs, with only weak expression observed in the alveolar regions (**Figure 2A–F**). In contrast, the lungs from BLM-treated mice exhibited pronounced CIRBP upregulation, particularly in regions with fibrosis (**Figure 2G–L**). This pattern was consistent with our previous observation of elevated CIRBP expression in the fibrotic regions of lung tissue from patients with IPF (11). These results indicate that CIRBP expression is globally upregulated in the context of pulmonary fibrosis compared to normal lungs, with particularly high expression in fibrotic regions. These findings suggest that CIRBP may be associated with fibrotic remodeling in the lung.

CIRBP-Induced Alterations in Gene Expression and Protein Production in Lung Fibroblasts

RNA-seq was performed to comprehensively analyze the mRNA expression profiles in primary lung fibroblasts isolated from WT mice, with or without stimulation by rmCIRBP. A volcano plot of the differentially expressed genes is shown in **Figure 3A**, and a heatmap of the representative genes exhibiting more than 2.5-fold change is shown in **Figure 3B**. The

rmCIRBP-stimulated fibroblasts exhibited marked changes in gene expression compared to unstimulated fibroblasts. Specifically, 630 mRNAs, 81 long non-coding RNAs (lncRNAs), and 2 non-coding RNAs (ncRNAs) were upregulated, whereas 385 mRNAs, 51 lncRNAs, and 4 ncRNAs were downregulated following rmCIRBP treatment.

Gene Ontology (GO) enrichment analysis revealed significant enrichment of GO terms associated with biological processes such as inflammation and immune responses (**Supplementary Figure 2A–B**; Additional file), molecular functions such as chemokine and cytokine activity (**Supplementary Figure 3A–B**; Additional file), and cellular components such as extracellular space and extracellular region (**Supplementary Figure 4A–B**; Additional file). Cytokine- and chemokine-related gene sets were highly expressed in rmCIRBP-stimulated lung fibroblasts (**Supplementary Figure 5**; Additional file). In contrast, the expression profiles of genes associated with the extracellular matrix (**Supplementary Figure 6**; Additional file) and growth factors (**Supplementary Figure 7**; Additional file) were variable, with both upregulated and downregulated genes showing no consistent trend.

To validate these transcriptomic findings, representative profibrotic proteins, cytokines, and growth factors were analyzed by qPCR, Western blotting, and ELISA. qPCR using mRNA extracted from rmCIRBP-stimulated fibroblasts revealed that the expression of *Acta2* was significantly upregulated compared with unstimulated controls, whereas *Fn1* showed no significant differences (**Figure 3C–D**). Western blot analysis of fibroblast lysates demonstrated that the intracellular protein levels of α-SMA and fibronectin were comparable between rmCIRBP-stimulated and control groups (**Figure 3E–F**). In parallel, ELISA of the culture supernatants showed that rmCIRBP stimulation did not significantly increase the levels of TGF-β, PDGF, IFN-γ, or IL-1β, whereas the concentrations of TNFα and IL-6 were significantly elevated, with IL-6 exhibiting a particularly pronounced increase (**Figure3G–L**).

Taken together, these results indicate that CIRBP does not directly enhance the intracellular expression of α-SMA or other profibrotic markers but instead promotes the production of inflammatory cytokines such as TNFα and IL-6.

Direct Effects of CIRBP on Lung Fibroblasts and the Inhibitory Role of C23

Primary lung fibroblasts isolated from WT mice were examined to investigate the functional effects of CIRBP on lung fibroblasts. Specifically, extracellular collagen production, cell proliferation, migratory ability, and collagen contraction capability were assessed. In addition, we compared fibroblasts treated with rmCIRBP alone to those treated with a combination of rmCIRBP and the CIRBP-derived peptide C23 to assess the therapeutic potential of C23. Treatment with rmCIRBP significantly increased the concentration of soluble extracellular collagen in the culture supernatant compared to the unstimulated controls, and this increase was attenuated by co-treatment with C23 (**Figure 4A**). Similarly, rmCIRBP stimulation enhanced lung fibroblast proliferation, an effect that was reduced following the addition of C23 (**Figure 4B**). In addition, rmCIRBP stimulation promoted fibroblast migration, which was also diminished by C23 treatment (**Figure 4C–D**). In contrast, rmCIRBP had no effect on the collagen contraction capability of lung fibroblasts (**Figure 4E–F**).

These findings suggest that while rmCIRBP does not directly promote fibroblast-to-myofibroblast differentiation or enhance cell contractility, it may contribute to fibrosis by increasing extracellular collagen secretion, fibroblast proliferation, and migration. C23 may inhibit fibrosis progression by suppressing these CIRBP-induced fibroblast functions.

TLR2/4-Dependent Regulation of IL-6 Production, Collagen Secretion, and Cell Proliferation by CIRBP in Lung Fibroblasts

According to the report by Bolourani et al., CIRBP is suggested to promote IL-6 expression in

lung fibroblasts through the TLR4 signaling pathway (17). Xiaoping Qiang et al. demonstrated that CIRBP exhibits high binding affinity to TLR4 and TLR2 (15). Therefore, in this study, we investigated whether CIRBP induces IL-6 production in lung fibroblasts via TLR4 and TLR2, explored the role of IL-6 in CIRBP-mediated extracellular collagen secretion and cell proliferation, and examined the effects of CIRBP-derived peptide C23 on these processes.

Primary lung fibroblasts derived from WT mice were treated with rmCIRBP, resulting in a significant increase in IL-6 protein levels in the culture supernatant compared to the control group. However, cotreatment with C23, a TLR4 inhibitor (TLR4-I), or a TLR2 inhibitor (TLR2-I) significantly suppressed this increase; the inhibitory effect was most pronounced with C23, followed by TLR4-I and TLR2-I (**Figure 5A**). These findings suggest that CIRBP-induced IL-6 production is mediated through the TLR4 and TLR2 pathways and that C23 may competitively inhibit the interaction between CIRBP and TLR4 and/or TLR2 signaling, thereby suppressing IL-6 induction.

Subsequently, an anti-IL-6 antibody was added, and its effects were assessed to investigate whether IL-6 mediates CIRBP-induced collagen secretion and cell proliferation. Cotreatment with the anti-IL-6 antibody significantly reduced soluble collagen levels and cell proliferation compared to rmCIRBP treatment alone (**Figure 5B–C**), indicating that autocrine IL-6 signaling contributes to the profibrotic effects of CIRBP on lung fibroblasts.

Next, we examined whether the effects of CIRBP on collagen secretion and proliferation were dependent on TLR4 and TLR2 signaling. Co-treatment with TLR4-I or TLR2-I significantly attenuated CIRBP-induced soluble collagen production and fibroblast proliferation compared to treatment with rmCIRBP alone (**Figures 5D–E**), further supporting the involvement of both receptors in mediating the fibrotic effects of CIRBP.

These results demonstrate that CIRBP promotes IL-6 production in lung fibroblasts via the TLR4 and TLR2 pathways, and the resulting autocrine IL-6 signaling enhances extracellular collagen secretion and cell proliferation (**Figure 5F**). Furthermore, C23 appears to competitively inhibit CIRBP signaling, thereby suppressing IL-6 production and potentially exerting antifibrotic effects.

Therapeutic Effect of C23 on BLM-Induced Pulmonary Fibrosis

We compared a C23-treated group with a placebo-treated group using the BLM-induced pulmonary fibrosis model to evaluate the therapeutic potential of C23 in pulmonary fibrosis (**Figure 6A**). The C23-treated mice showed significantly improved survival compared to the placebo-treated group following BLM administration (**Figure 6B**). Histological assessment of lung tissues on day 21 revealed that pulmonary fibrosis was markedly attenuated in the C23-treated group, as indicated by a significant reduction in the Ashcroft scores (**Figure 6C**). The lung hydroxyproline content was also significantly decreased in the C23-treated group compared to the placebo group (**Figure 6D**). Western blot analysis showed that the expression levels of CIRBP, α-SMA, and fibronectin were significantly reduced in the lungs of C23-treated mice compared to those of the placebo-treated mice (**Figures 6E–G**).

Collectively, these results demonstrate that the therapeutic administration of C23 effectively attenuates pulmonary fibrosis in the BLM-induced mouse model, supporting its potential as a therapeutic agent for fibrotic lung disease.

DISCUSSION

In this study, we demonstrated that CIRBP contributes to the progression of pulmonary fibrosis and may serve as a therapeutic target. In a BLM-induced fibrosis model, *CIRBP*-deficient mice showed significantly reduced fibrosis and improved survival compared to WT

mice. CIRBP expression was notably upregulated in the fibrotic lesions of BLM-treated WT mice. In vitro, rmCIRBP promoted IL-6 production, cell proliferation, migration, and collagen production in lung fibroblasts, and these effects were suppressed by TLR2/4 inhibitors, anti-IL-6 antibodies, and the CIRBP-derived peptide C23. These findings suggest a novel mechanism where elevated CIRBP in fibrotic lungs induces IL-6 via TLR2/4 in fibroblasts, leading to autocrine activation and fibrosis progression. Furthermore, C23 treatment suppressed fibrosis and improved survival in WT mice, supporting the potential of CIRBP pathway inhibition as a new therapeutic strategy for pulmonary fibrosis.

CIRBP is known to be upregulated in response to various stress stimuli, including cold, UV radiation, hypoxia, oxidative stress, and glucose deprivation (18, 19). Once expressed, CIRBP translocates from the nucleus to the cytoplasm, where it binds to the 3′ untranslated region of target mRNAs to regulate their stability and translation (20). Through these functions, intracellular CIRBP contributes to suppressing apoptosis and enhancing antioxidant responses and may act as a tumor-promoting factor (9). Under stress conditions, overexpressed CIRBP may be secreted into the extracellular space via nonclassical pathways, such as lysosomal secretion and exosomes (9, 21). In addition, in pathological conditions such as hemorrhagic shock or sepsis, CIRBP may leak into the extracellular space due to cellular injury (15). In the present study, western blot analysis demonstrated that CIRBP expression was significantly upregulated in the lungs of BLM-treated mice compared to controls, with particularly strong expression in fibrotic lesions, providing novel insights into the involvement of CIRBP in fibrotic lung pathology. Our previous study also identified high CIRBP expression, specifically in fibrotic regions of lung tissues from patients with IPF (11). Various forms of cellular stress have been reported to be involved within the lung tissue in pulmonary fibrosis. Based on these reports and the findings of our previous and current studies, we suggest that CIRBP expression is upregulated in response to cellular stress in

diseased lung tissue, potentially leading to its high expression within the tissue and substantial release into the extracellular space.

Extracellular CIRBP has been shown to act as a DAMP, primarily activating innate immune responses by binding to receptors such as TLR4–MD2 and TREM-1, thereby promoting the production of proinflammatory cytokines and amplifying the inflammatory response in sepsis (15, 22). Thus, CIRBP exhibits dual functionality; it contributes to stress responses and cytoprotection intracellularly and serves as a proinflammatory mediator extracellularly, with its role largely dependent on its cellular localization. Recent attention has focused on the role of DAMPs in promoting fibrotic processes through the activation of innate immunity in pulmonary fibrosis (6, 7). In our previous study, we reported that elevated serum CIRBP levels in patients with IPF were associated with disease progression and poor prognosis, suggesting that stress-induced extracellular CIRBP may contribute to fibrosis in the lung (11). Based on this background, the present study aimed to clarify the role of CIRBP in pulmonary fibrosis. Although Bolourani et al. demonstrated that *CIRBP* deficiency or pharmacological inhibition by the CIRBP-derived peptide C23 attenuated BLM-induced pulmonary fibrosis, their study employed a nonstandard subcutaneous administration route and did not assess the survival outcomes (17). In contrast, our study employed the more widely recommended BLM model via IT administration using the OA method and clearly demonstrated, for the first time that both genetic deletion of *CIRBP* and therapeutic intervention with C23 could suppress fibrosis and improve survival. These findings provide compelling evidence that CIRBP functions as a profibrotic factor, particularly when overexpressed; furthermore, CIRBP inhibition can effectively reduce fibrotic progression and improve survival in pulmonary fibrosis.

Another strength of the current study lies in elucidating the pathophysiological role of CIRBP via in vivo analyses and at the cellular level via in vitro experiments. Stimulation of

lung fibroblasts with CIRBP enhanced collagen production, cell proliferation, and migration, whereas it did not affect collagen gel contraction or induce significant changes in the protein expression of classical myofibroblast markers such as α-SMA. Taken together, these findings suggest that CIRBP promotes selected functional aspects of fibroblast activation but is unlikely to act as a direct driver of complete myofibroblast differentiation. In our in vitro experiments, rmCIRBP stimulation significantly increased *Acta2* mRNA expression in primary lung fibroblasts; however, this transcriptional change was not accompanied by a corresponding increase in α-SMA protein levels. Such discrepancies between mRNA and protein expression may reflect post-transcriptional regulation, delayed protein synthesis, or the requirement for additional profibrotic stimuli. Alternatively, the difference in stimulation duration—24 hours for mRNA analysis versus 5 days for protein assessment—may capture distinct phases of the fibroblast response to CIRBP. Furthermore, RNA-seq analysis revealed that CIRBP stimulation induced the expression of numerous cytokine- and chemokine-related gene clusters. ELISA also confirmed increased secretion of representative cytokines, such as IL-6 and TNF-α. IL-6 is known to be involved in the pathogenesis of tissue fibrosis (23, 24). Previous studies have reported that IL-6 stimulation induces collagen production in fibroblasts (25, 26), and IL-6 secreted by lung fibroblasts promotes their proliferation (27). Consistently, in the present study, the addition of anti-IL-6 antibodies significantly suppressed CIRBP-induced collagen production and cell proliferation, indicating that autocrine IL-6 induced by CIRBP contributes to the activation of lung fibroblasts. Moreover, the addition of TLR2 and TLR4 inhibitors suppressed CIRBP-induced IL-6 production, collagen synthesis, and cell proliferation, suggesting that these effects are mediated via TLR signaling pathways. Although previous studies have shown that CIRBP can bind to both TLR4 and TLR2 (15), the functional relevance of this interaction was primarily evaluated in relation to TLR4 (12, 17). The current study is significant in that it demonstrates that CIRBP activates fibroblasts not

only via TLR4 but also via TLR2, thereby providing a more comprehensive understanding of the mechanisms by which CIRBP contributes to the development of pulmonary fibrosis.

C23 is a short peptide derived from CIRBP and is thought to suppress its function by competitively inhibiting the binding between CIRBP and its target molecules. In vivo and in vitro analyses demonstrated that C23 inhibits fibroblast activation by blocking CIRBP-induced IL-6 signaling via TLR2/4, suggesting its potential to attenuate pulmonary fibrosis. Anti-IL-6 antibodies are currently approved for autoimmune diseases, such as rheumatoid arthritis and systemic sclerosis (28), and the findings of the present study suggest their possible efficacy in secondary pulmonary fibrosis associated with these conditions. However, directly targeting IL-6 requires careful consideration of infection risk because it plays a critical role in innate and adaptive immunity (29). IPF, the most typical form of pulmonary fibrosis, carries a high risk of respiratory infections. Recurrent infections are linked to functional decline and increased risk of acute exacerbation (AE-IPF) (30), and immunosuppressive therapy is associated with poor outcomes (31). Therefore, anti-IL-6 therapy should be used cautiously in patients with pulmonary fibrosis, except in cases with autoimmune features. In contrast, C23, or a neutralizing anti-CIRBP antibody, may suppress IL-6 production under fibrotic conditions by inhibiting the interaction between CIRBP and TLR2/4. Unlike anti-IL-6 antibodies, which directly neutralize IL-6, CIRBP-targeted therapies act upstream by disrupting the CIRBP–TLR2/4 interaction, selectively reducing IL-6 production in fibrotic settings. This indirect modulation may allow for the attenuation of fibrosis progression while preserving essential IL-6-mediated immune responses, potentially offering clinical benefits. Thus, CIRBP may represent a novel therapeutic target for pulmonary fibrosis; further studies are warranted to validate its efficacy.

This study has several limitations. First, while we focused on the role of CIRBP in lung fibroblasts, its involvement in pulmonary fibrosis through nonfibroblast populations, such as

epithelial or immune cells, was not explored and remains an important subject for future investigations. Second, although CIRBP-induced IL-6 production and fibroblast activation were significantly suppressed by TLR2/4 inhibitors and C23, the inhibition was incomplete, suggesting the possible involvement of additional TLR-independent pathways, which should be examined in the future. Third, because our in vitro experiments were performed in monoculture, these findings mainly support an autocrine effect of IL-6 in fibroblasts. However, in the in vivo fibrotic environment, various immune and structural cells also produce IL-6, suggesting that paracrine IL-6 signaling may additionally contribute to fibroblast activation. Fourth, the clinical relevance of the CIRBP-TLR-IL-6 axis in patients with pulmonary fibrosis has not been fully established. Further validation using patient-derived samples and future clinical studies will be necessary to clarify its significance and therapeutic potential in human disease.

In conclusion, this study demonstrated that CIRBP contributes to the progression of pulmonary fibrosis by promoting IL-6 production via TLR4 and TLR2 signaling, thereby enhancing fibroblast proliferation, migration and collagen production. Furthermore, the CIRBP-derived peptide C23 suppressed these responses and exerted antifibrotic effects. In the BLM-induced pulmonary fibrosis mouse model, targeting CIRBP attenuated fibrotic changes in the lung and significantly improved survival. These findings support the potential of the CIRBP-TLR-IL-6 axis as a novel therapeutic target and suggest that CIRBP may serve as a promising candidate for treating pulmonary fibrosis.

Acknowledgments: The authors thank Enago (www.enago.jp) for the English language review. Part of this work was conducted at the Advanced Research Facilities & Services, Hamamatsu University School of Medicine. We sincerely thank Asuka Miyagi and Ryo Horiguchi for their invaluable assistance.

Author contributions

YM: Conception and design, data collection, data analysis and interpretation, manuscript writing. HH: Conception and design, data collection, data analysis and interpretation, manuscript writing, and final approval of the manuscript. AF, HW, HN, YI, HY, YS, MK, KF, NE, TF and NI: Data collection, data analysis, and supervision. TS: Conception and design, manuscript writing, and administrative support.

Role of funding source: This study was supported by a grant from the Japan Society for the Promotion of Science (21K08176 to H.H.), a grant from the TERUMO LIFE SCIENCE FOUNDATION (22-III 4014 to H.H.), and a HUSM Grant-in-Aid. The funding source did not provide any input or contributions in the development of the research or manuscript.

Conflicts of interest: The authors declare that no competing interests exist.

Availability of data and materials: The data that support the findings of this study are available from the corresponding authors upon reasonable request. The RNA-seq data generated in this study have been deposited in the Gene Expression Omnibus (GEO) under accession number GSE294583 (https://www.ncbi.nlm.nih.gov/geo/query/acc.cgi?acc=GSE294583). The data can be accessed with the following token: kfityyewrncrvir during peer review.

Declaration of Generative AI and AI-assisted technologies in the writing process

None of Generative AI and AI-assisted technologies were used in this manuscript.

References

1. Raghu G, Remy-Jardin M, Richeldi L, Thomson CC, Inoue Y, Johkoh T, et al. Idiopathic Pulmonary Fibrosis (an Update) and Progressive Pulmonary Fibrosis in Adults: An Official ATS/ERS/JRS/ALAT Clinical Practice Guideline. Am J Respir Crit Care Med 2022; 205: e18-e47.

2. Rajan SK, Cottin V, Dhar R, Danoff S, Flaherty KR, Brown KK, et al. Progressive pulmonary fibrosis: an expert group consensus statement. Eur Respir J 2023; 61.

3. Popper H, Stacher-Priehse E, Brcic L, Nerlich A. Lung fibrosis in autoimmune diseases and hypersensitivity: how to separate these from idiopathic pulmonary fibrosis. Rheumatol Int 2022; 42: 1321-1330.

4. Lederer DJ, Martinez FJ. Idiopathic Pulmonary Fibrosis. N Engl J Med 2018; 378: 1811-1823.

5. Wijsenbeek M, Cottin V. Spectrum of Fibrotic Lung Diseases. N Engl J Med 2020; 383: 958-968.

6. Desai O, Winkler J, Minasyan M, Herzog EL. The Role of Immune and Inflammatory Cells in Idiopathic Pulmonary Fibrosis. Front Med (Lausanne) 2018; 5: 43.

7. Ellson CD, Dunmore R, Hogaboam CM, Sleeman MA, Murray LA. Danger-associated molecular patterns and danger signals in idiopathic pulmonary fibrosis. Am J Respir Cell Mol Biol 2014; 51: 163-168.

8. Corre M, Lebreton A. Regulation of cold-inducible RNA-binding protein (CIRBP) in response to cellular stresses. Biochimie 2024; 217: 3-9.

9. Liao Y, Tong L, Tang L, Wu S. The role of cold-inducible RNA binding protein in cell stress response. Int J Cancer 2017; 141: 2164-2173.

10. Zhong P, Zhou M, Zhang J, Peng J, Zeng G, Huang H. The role of Cold-Inducible RNA-binding protein in respiratory diseases. J Cell Mol Med 2022; 26: 957-965.

11. Hozumi H, Kataoka K, Kondoh Y, Isayama T, Okada J, Sugiura K, et al. Clinical Significance of Cold-Inducible RNA-Binding Protein in Idiopathic Pulmonary Fibrosis. Chest 2021; 160: 2149-2157.

12. Bolourani S, Sari E, Brenner M, Wang P. The role of eCIRP in bleomycin-induced pulmonary fibrosis in mice. PLoS One 2022; 17: e0266163.

13. Jenkins RG, Moore BB, Chambers RC, Eickelberg O, Königshoff M, Kolb M, et al. An Official American Thoracic Society Workshop Report: Use of Animal Models for the Preclinical Assessment of Potential Therapies for Pulmonary Fibrosis. Am J Respir Cell Mol Biol 2017; 56: 667-679.

14. Masuda T, Itoh K, Higashitsuji H, Higashitsuji H, Nakazawa N, Sakurai T, et al. Cold-inducible RNA-binding protein (Cirp) interacts with Dyrk1b/Mirk and promotes proliferation of immature male germ cells in mice. Proc Natl Acad Sci U S A 2012; 109: 10885-10890.

15. Qiang X, Yang WL, Wu R, Zhou M, Jacob A, Dong W, et al. Cold-inducible RNA-binding protein (CIRP) triggers inflammatory responses in hemorrhagic shock and sepsis. Nat Med 2013; 19: 1489-1495.

16. Ashcroft T, Simpson JM, Timbrell V. Simple method of estimating severity of pulmonary fibrosis on a numerical scale. J Clin Pathol 1988; 41: 467-470.

17. Bolourani S, Sari E, Brenner M, Wang P. Extracellular CIRP Induces an Inflammatory Phenotype in Pulmonary Fibroblasts via TLR4. Front Immunol 2021; 12: 721970.

18. Nishiyama H, Itoh K, Kaneko Y, Kishishita M, Yoshida O, Fujita J. A glycine-rich RNA-binding protein mediating cold-inducible suppression of mammalian cell growth. J Cell Biol 1997; 137: 899-908.

19. Danno S, Nishiyama H, Higashitsuji H, Yokoi H, Xue JH, Itoh K, et al. Increased transcript level of RBM3, a member of the glycine-rich RNA-binding protein family, in human cells

in response to cold stress. Biochem Biophys Res Commun 1997; 236: 804-807.

20. Xue JH, Nonoguchi K, Fukumoto M, Sato T, Nishiyama H, Higashitsuji H, et al. Effects of ischemia and H2O2 on the cold stress protein CIRP expression in rat neuronal cells. Free Radic Biol Med 1999; 27: 1238-1244.

21. Qu Y, Dubyak GR. P2X7 receptors regulate multiple types of membrane trafficking responses and non-classical secretion pathways. Purinergic Signal 2009; 5: 163-173.

22. Denning NL, Aziz M, Murao A, Gurien SD, Ochani M, Prince JM, et al. Extracellular CIRP as an endogenous TREM-1 ligand to fuel inflammation in sepsis. JCI Insight 2020; 5.

23. She YX, Yu QY, Tang XX. Role of interleukins in the pathogenesis of pulmonary fibrosis. Cell Death Discov 2021; 7: 52.

24. Li Y, Zhao J, Yin Y, Li K, Zhang C, Zheng Y. The Role of IL-6 in Fibrotic Diseases: Molecular and Cellular Mechanisms. Int J Biol Sci 2022; 18: 5405-5414.

25. Duncan MR, Berman B. Stimulation of collagen and glycosaminoglycan production in cultured human adult dermal fibroblasts by recombinant human interleukin 6. J Invest Dermatol 1991; 97: 686-692.

26. Le TT, Karmouty-Quintana H, Melicoff E, Le TT, Weng T, Chen NY, et al. Blockade of IL-6 Trans signaling attenuates pulmonary fibrosis. J Immunol 2014; 193: 3755-3768.

27. Fries KM, Felch ME, Phipps RP. Interleukin-6 is an autocrine growth factor for murine lung fibroblast subsets. Am J Respir Cell Mol Biol 1994; 11: 552-560.

28. Narazaki M, Kishimoto T. Current status and prospects of IL-6-targeting therapy. Expert Rev Clin Pharmacol 2022; 15: 575-592.

29. Hunter CA, Jones SA. IL-6 as a keystone cytokine in health and disease. Nat Immunol 2015; 16: 448-457.

30. Molyneaux PL, Maher TM. The role of infection in the pathogenesis of idiopathic pulmonary fibrosis. Eur Respir Rev 2013; 22: 376-381.

31. Raghu G, Anstrom KJ, King TE, Jr., Lasky JA, Martinez FJ. Prednisone, azathioprine, and N-acetylcysteine for pulmonary fibrosis. N Engl J Med 2012; 366: 1968-1977.

FIGURE LEGENDS

Figure 1. *CIRBP* deficiency attenuates bleomycin (BLM)-induced pulmonary fibrosis and improves survival.

(A) Experimental scheme of the BLM-induced pulmonary fibrosis model using wild-type (WT) and *CIRBP* knockout (*CIRBP*$^{-/-}$) mice.

(B) Kaplan–Meier survival curves after BLM instillation.

(C) Representative images of lung tissues stained with Masson's trichrome on day 21. Scale bars: 200 μm. Quantification of fibrosis severity using Ashcroft scores (n = 9 per group).

(D) Hydroxyproline content in the left lung lobes as a measure of collagen deposition (n = 5).

(E–G) Western blot analysis of CIRBP, α-SMA, and fibronectin expression in the lung homogenates. Densitometric quantification of the western blot signals normalized to β-actin. Data are shown as mean ± the standard error of the mean (SEM). *P < 0.05 using one-way ANOVA and Tukey's multiple comparison or log-rank test.

Figure 2. CIRBP expression is increased in fibrotic lung regions and localized to fibrotic lesions.

(A–C) Masson's trichrome staining, CIRBP immunostaining, and isotype IgG staining of lungs from PBS-treated mice, respectively. Scale bar = 1,000 μm.

(D–F) Magnified views of the black squares shown in images A, B, and C, respectively. CIRBP was mainly expressed around the airways in the control lungs, with only weak expression observed in the alveolar regions. Scale bar = 200 μm

(G–I) Masson's trichrome staining, CIRBP immunostaining , and isotype IgG staining of lungs from BLM-treated mice, respectively. Scale bar = 1,000 μm.

(J–L) Magnified views of the black squares shown in images G, H, and I, respectively. CIRBP expression was markedly upregulated in the fibrotic lesions of BLM-treated lungs and colocalized in the regions of collagen deposition. Scale bar = 200 μm.

Figure 3. Transcriptomic profiling and cytokine production in CIRBP-stimulated primary mouse lung fibroblasts.

(A) Volcano plot of differentially expressed genes in fibroblasts treated with rmCIRBP vs. control.

(B) Heatmap of representative upregulated and downregulated genes (fold change >2.5).

(C–D) Quantitative PCR analysis of *Acta2* and *Fn1* mRNA expression in fibroblasts treated with or without rmCIRBP. TGF-β–stimulated fibroblasts were included as a positive control.

(E–F) Western blot analysis of α-SMA and fibronectin protein expression in fibroblasts treated with or without rmCIRBP. TGF-β–stimulated fibroblasts were included as a positive control.

(G–L) ELISA quantification of cytokines in the culture supernatants: TGF-β, PDGF, IFN-γ, IL-1β, TNF-α, and IL-6.

Data are presented as mean ± SEM. *P < 0.05 using one-way ANOVA and Tukey's multiple comparison test.

rmCIRBP, recombinant mouse CIRBP.

Figure 4. CIRBP promotes collagen secretion and fibroblast proliferation in vitro, and C23 suppresses these activities.

(A) Soluble collagen concentration in the culture supernatant of primary lung fibroblasts treated with rmCIRBP and/or C23 for 5 days, as measured using the Sircol assay. TGF-β treatment served as a positive control.

(B) Proliferative capacity of primary lung fibroblasts assessed by a water-soluble tetrazolium salt (WST)-based colorimetric assay (Cell Counting Kit-8) at 24 and 48 h after treatment with rmCIRBP and/or C23. PDGF treatment served as a positive control.

(C) Representative phase-contrast images of wound areas at 0 h (upper panels) and 24 h after treatment initiation (lower panels) in primary mouse lung fibroblasts treated with rmCIRBP and/or C23. TGF-β treatment served as a positive control.

(D) Quantification of wound closure (%) at 24 h relative to the initial wound area in primary mouse lung fibroblasts treated with rmCIRBP and/or C23. TGF-β treatment served as a positive control.

(E) Representative images of collagen gel contraction in primary mouse lung fibroblasts treated with rmCIRBP and/or C23. TGF-β treatment served as a positive control.

(F) Contraction index calculated as the percentage of the initial gel area after 24 hours in primary mouse lung fibroblasts treated with rmCIRBP and/or C23. TGF-β treatment served as a positive control.

Data are shown as mean ± SEM. *$P < 0.05$ using one-way ANOVA and Tukey's multiple comparison test.

rmCIRBP, recombinant mouse CIRBP.

Figure 5. CIRBP promotes collagen production and proliferation via TLR2/4-dependent IL-6 signaling.

(A) IL-6 concentrations in the culture supernatants of primary lung fibroblasts treated with rmCIRBP, with or without C23, TLR4-I, or TLR2-I, measured by ELISA.

(B) Soluble collagen levels in the supernatants following treatment with rmCIRBP ± anti-IL-6 antibody.

(C) Proliferative activity of fibroblasts assessed by the WST assay after treatment with

rmCIRBP and/or anti-IL-6 antibody.

(D) Soluble collagen production in fibroblasts treated with rmCIRBP and either TLR4-I or TLR2-I.

(E) Fibroblast proliferation measured using the WSTT assay following cotreatment with rmCIRBP and TLR4-I or TLR2-I.

(F) Schematic representation of the proposed mechanism: CIRBP, which is highly expressed in fibrotic lungs, stimulates IL-6 production via TLR2/4, promoting collagen secretion and fibroblast proliferation in an autocrine manner and contributing to the progression of tissue fibrosis.

Data are presented as mean ± SEM. *P < 0.05 using one-way ANOVA and Tukey's multiple comparison test.

Figure 6. Therapeutic administration of the C23 peptide suppresses pulmonary fibrosis and improves survival.

(A) Experimental timeline for BLM and C23 treatment. C23 was administered intraperitoneally once daily on days 7–11 and 14–18.

(B) Kaplan–Meier survival analysis showing improved outcomes in C23-treated mice (n = 10).

(C) Masson's trichrome staining of lung sections on day 21 (n = 10).

(D) Hydroxyproline content in the left lung lobes as a measure of collagen deposition (n = 10).

(E–G) Western blot analysis of CIRBP, α-SMA, and fibronectin expression in the lung homogenates.

*P < 0.05 using one-way ANOVA and Tukey's multiple comparison or log-rank test. Data are shown as mean ± SEM.

Figure 1

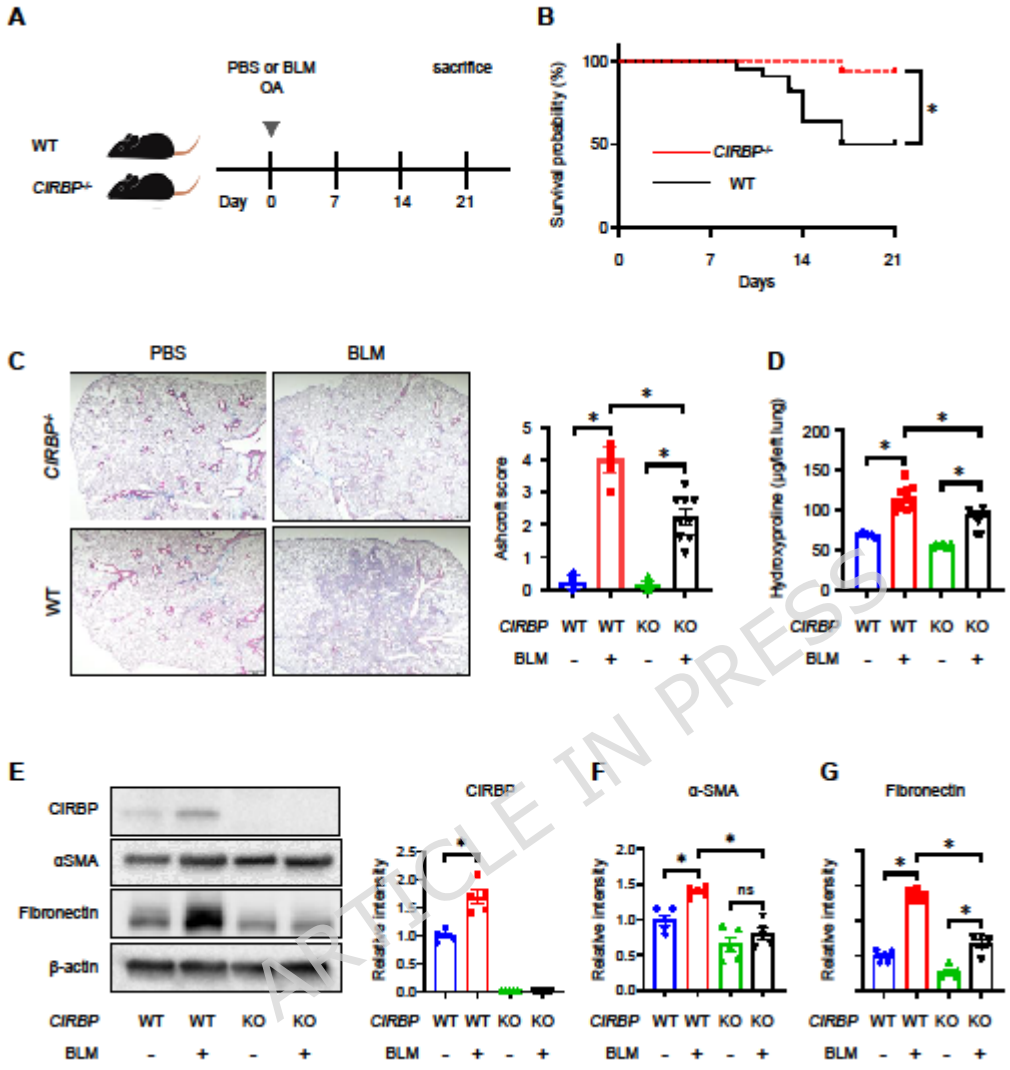

Figure 2

Immunostaining of CIRBP Expression in mouse lung

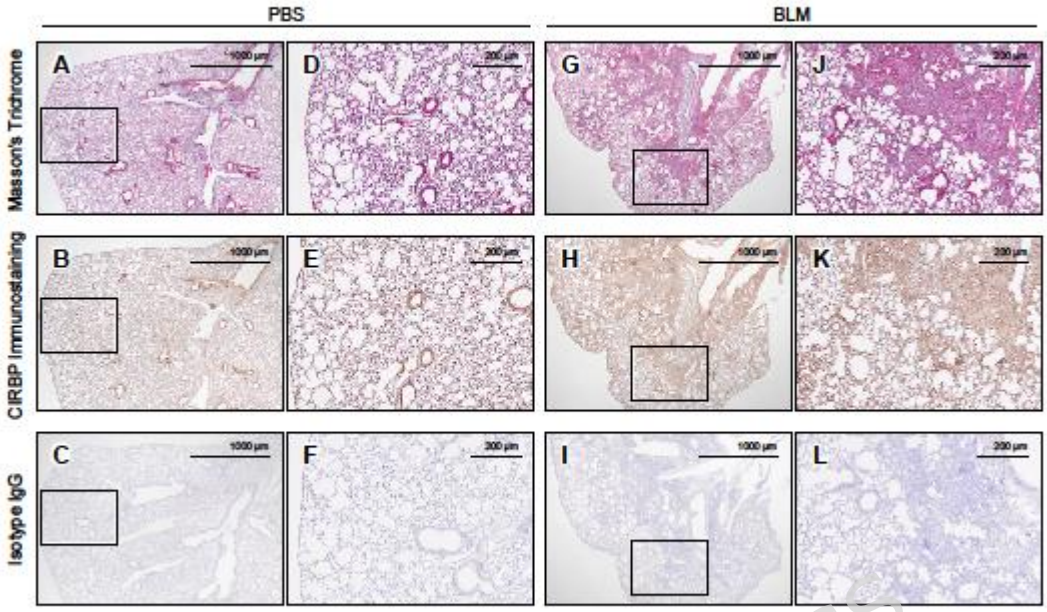

Figure 3

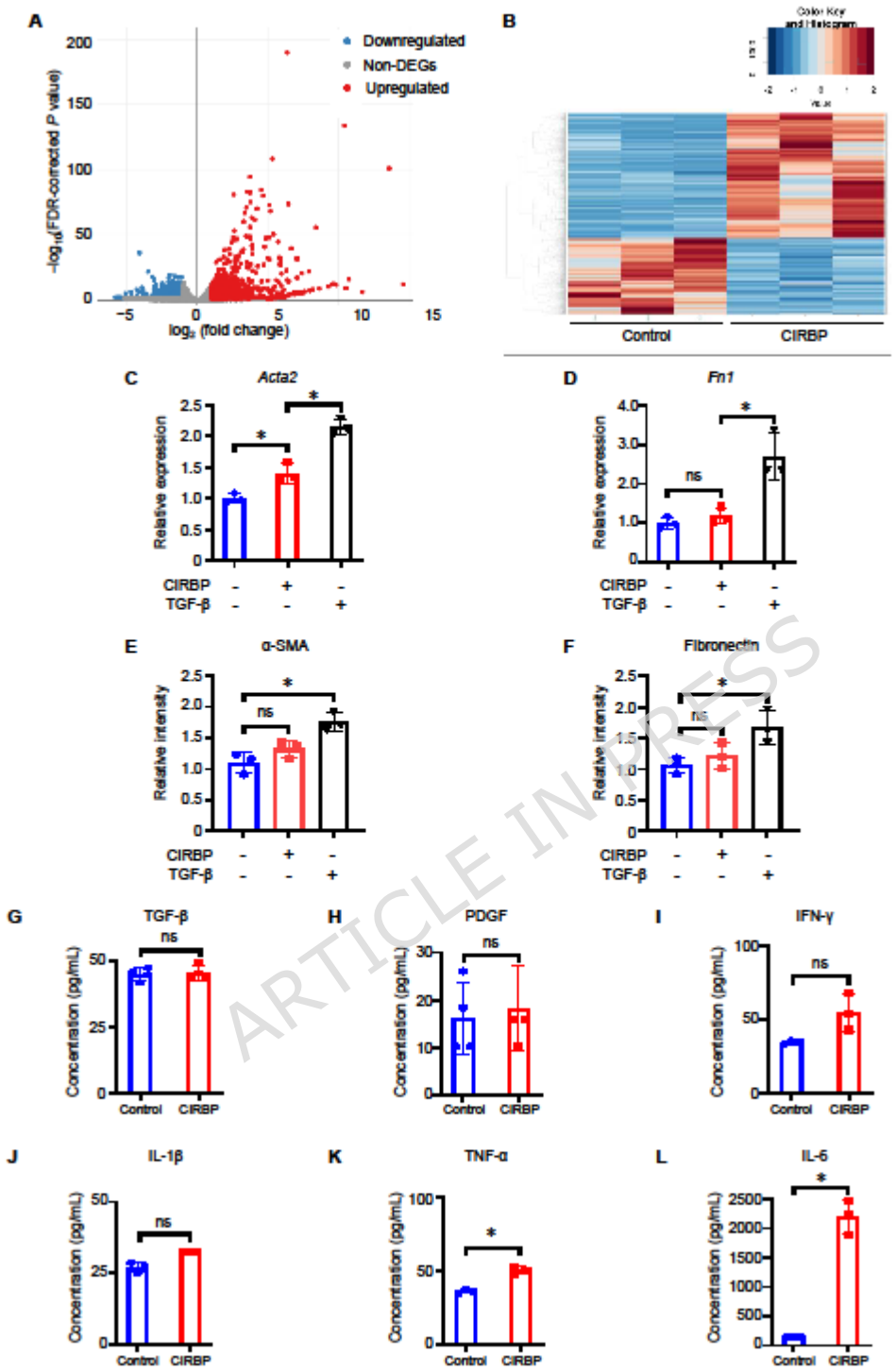

Figure 4

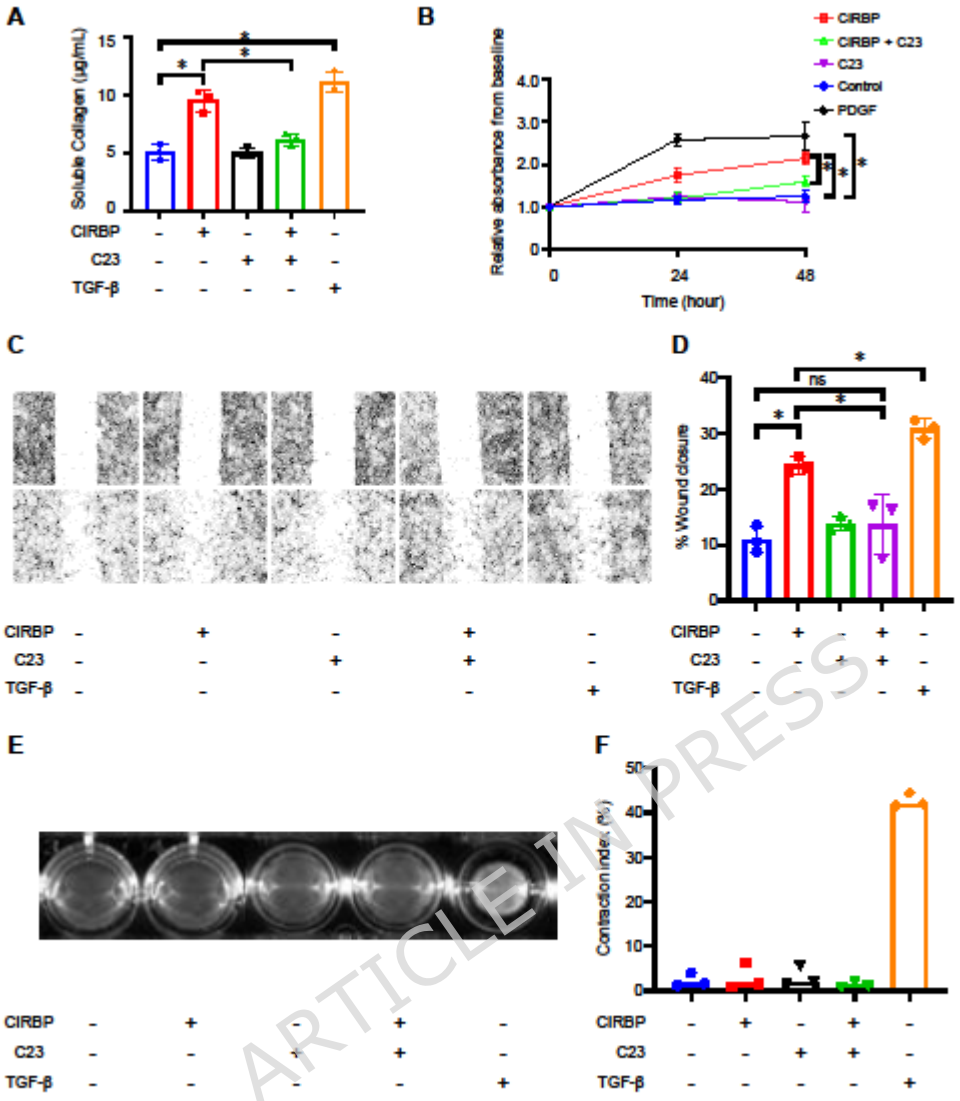

Figure 5